Power Decoupling Methods for Grid Support Provided by Ultra-Fast Bidirectional Chargers

IEEE Open Journal of
Industry Applications

Received 8 August 2024; revised 12 November 2024; accepted 5 January 2025. Date of publication 14 January 2025;
date of current version 20 February 2025.

Digital Object Identifier 10.1109/OJIA.2025.3529042

Power Decoupling Methods for Grid Support Provided by Ultra-Fast Bidirectional Chargers

ALESSANDRO ROVERI (Student Member, IEEE), VINCENZO MALLEMACI (Member, IEEE), FABIO MANDRILE (Member, IEEE), AND RADU BOJOI (Fellow, IEEE)

[1]Prima Electro S.p.A., 10024 Moncalieri, Italy
[2]Dipartimento Energia, Politecnico di Torino, 10129 Torino, Italy

CORRESPONDING AUTHOR: VINCENZO MALLEMACI (e-mail: vincenzo.mallemaci@polito.it)

This work was supported in part by the Project ROCKET (Reliable pOwer to Cloud multiKilowatt ElecTronics) and in part by the Piedmont Region, in the framework Programma Pluriennale Attività Produttive 2018/2020 Misura "Contratto di Insediamento".

ABSTRACT The installation of ultra-fast dc charging infrastructures is rapidly increasing worldwide in response to the exponential growing trend of electric vehicle (EV) market. Due to their discontinuous and unpredictable high power absorption, ultra-fast dc chargers pose a challenge for the power system stability. However, their negative impact on the grid operation can be mitigated by making them bidirectional, leveraging the energy stored in EV batteries or in the installed separate storage. Therefore, the power system can exploit this amount of energy to deal with unexpected grid large power imbalances. Moreover, ultra-fast dc chargers can contribute to power system stability by embedding virtual synchronous machine (VSM) algorithms into their ac/dc stage, i.e., the active front-end (AFE) converter unit. The charging station is thus enabled to provide grid services normally in charge of traditional synchronous generators, such as inertial behavior and short circuit current injection during faults to trigger line protections. However, the provision of inertial active power involves a non-negligible reactive power contribution due to the active-reactive power coupling, thus increasing the output current of the converter. Nevertheless, the power coupling also affects the grid support during faults. Indeed, when the AFE injects a short circuit current into the grid, a fluctuating active power can propagate from the grid to the EVs, resulting in a potential cause of degradation for the EV batteries. Therefore, this article proposes a feedforward-based decoupling solution to guarantee the complete active–reactive power dynamic decoupling while the AFE of an ultra-fast dc charger is providing grid support. Moreover, the proposed method ensures a full-decoupled dynamic response also in case of power references variation during the normal EV charging operation. The proposed decoupling algorithm is experimentally validated on a down-scaled 15 kVA two-level three-phase inverter, emulating the AFE of the ultra-fast dc charger.

INDEX TERMS Active front-ends (AFEs), electric vehicles (EVs), grid services, grid support, power decoupling, power system stability, ultra-fast dc chargers, virtual synchronous machines (VSMs).

I. INTRODUCTION

In recent years, governmental targeted policies are boosting the worldwide installation of public charging stations to keep pace with electric vehicle (EV) market. The global number of charging points increased by 40% between 2022 and 2023 and an exponential growing trend is still expected in the coming years. Indeed, public charging needs to increase sixfold by 2035 to reach the expected EV deployment levels [1]. Among the EV charging systems, on-board ac chargers have limited power ratings ($\leq$22 kW), being suitable for overnight charging. On the other hand, high-power off-board dc chargers have higher power ratings, in the range of 50–150 kW. These chargers directly deliver dc current to the battery pack through a galvanic insulated power converter installed outside the EV. The newest generations of ultra-fast dc chargers rated at 350 kW and above [2], [3] will guarantee an EV refueling time similar to that of gasoline cars, thus enabling faster and longer journeys

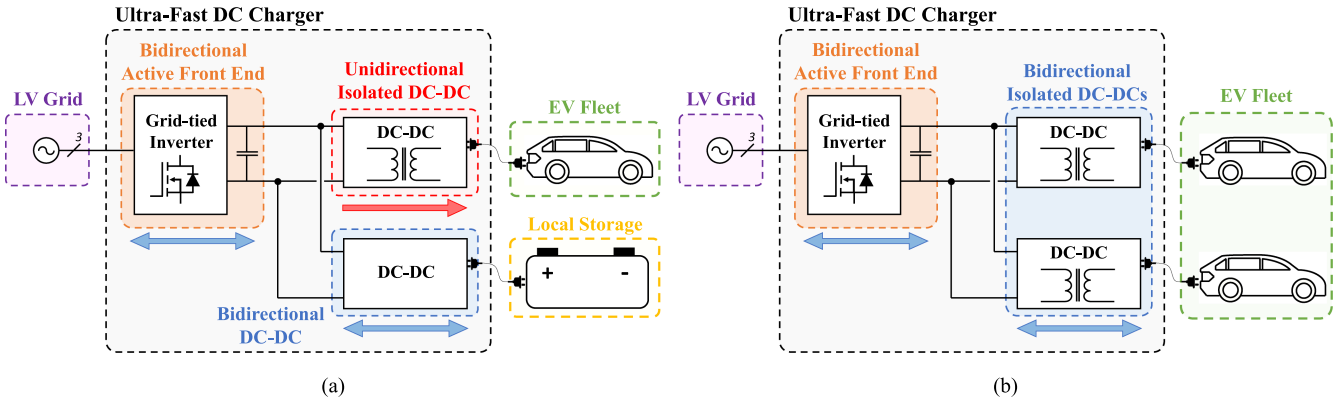

FIGURE 1. Simplified schemes of different bidirectional ultra-fast charging configurations with single bidirectional AFE unit. (a) The installed local storage is interfaced with a bidirectional dc/dc, while the dc/dc modules dedicated to EVs charging are kept unidirectional to reduce hardware requirements. (b) Bidirectional dc/dc converters supply EV batteries are connected to the distributed dc stage by means of bidirectional dc/dc modules, thus enabling the vehicle to grid (V2G) feature.

with EVs and encouraging mass-market consumers switch to electric [4].

Ultra-fast dc chargers are high-power loads, whose discontinuous and unpredictable operation poses a challenge for the power system stability. However, EV batteries and local storage installed inside the fast-charging stations can represent an energy reserve for the power system useful to deal with unexpected large imbalances between the power demand and generation [5], [6]. Therefore, most of the stability issues can be addressed by placing at the disposal of electrical system this amount of stored energy. As shown in the ultra-fast charger design options of Fig. 1, the reverse power flow can be enabled by interfacing the installed local storage [see Fig. 1(a)] or the EVs [see Fig. 1(b)] with bidirectional dc/dcs and making bidirectional the ac/dc power converter stage [i.e., the active front-end (AFE)] as well [4], [5], [7]. Furthermore, the bidirectional power converters' design combined with available stored energy opens up the possibility to make grid-connected ultra-fast chargers able to contribute to power system stability by providing ancillary services [8], [9], such as primary frequency regulation [10], [11], [12], voltage regulation [11], [12], [13], [14], inertial behavior [10], [11], [12], [13], grid support during faults [13], harmonic compensation [12], [13] and islanding capabilities [10].

Indeed, recent papers [10], [11], [12], [13] demonstrated that a charging station can fulfill both the charging process and the provision of grid services by embedding the virtual synchronous machine (VSM) algorithm into the bidirectional AFE control. The VSM concept is a valid solution to make grid-tied inverters behave as conventional synchronous generators (SGs) and ensuring immediate support to the grid also during fast transient events, such as frequency variations or voltage dips and swells. Although the VSM models proposed in the literature [15], [16] were mainly developed for renewable generation systems (i.e., photovoltaic and wind power plants), a VSM algorithm can be exploited in ultra-fast chargers as an add-on feature to minimize their impact on the grid. For example, in case of grid frequency variation, the AFE can inject/absorb active power by emulating the inertial behavior of SGs, thus limiting the grid frequency deviation. Instead, during voltage dips, it can provide reactive short circuit current to trigger the line protections, thus assisting the power system in faulty branches isolation and recovery of normal operating conditions [8], [9], [17]. While the VSM integration into ultra-fast chargers control makes them more grid friendly, the provision of ancillary services can represent an additional remuneration source for charging station operators, which is achieved by exploiting the installed hardware, after mutual agreement with the power system operator [5], [18], [19], [20]. The charging operation is the core functionality of the infrastructure, while ancillary services are just add-on features, which should impact as little as possible on the hardware design.

The provision of ancillary services through ultra-fast charging stations inherently involves the engagement of new stakeholders for grid support, such as station operators, EV owners, as well as the distribution system operators (DSOs). Indeed, ultra-fast dc chargers are normally connected to the low-voltage (LV) grid (see Fig. 1), thus taking advantage of the wide availability and reliability of LV industrial power electronics. Therefore, according to recent European directives [21], [22] and studies in the literature regarding distribution systems and distributed generation [23], [24], the DSOs will have to assist the transmission system operator in procuring ancillary services to ensure grid safe operation, by enabling also LV users, such as fast-charging hubs, to participate in ancillary services markets.

Nevertheless, the control algorithms designed for grid-forming power converters (i.e., VSMs) assume that the active power depends linearly only on the load angle (P-δ), while the reactive power only depends on the voltage amplitude (Q-V) [25]. This assumption is based on a purely inductive transmission line and a small load angle. However, in many cases (e.g., low voltage networks and microgrids), the grid

and VSM resistances and the load angle are not negligible. Consequently, the active and reactive power are coupled (i.e., when the active power varies, the reactive power changes as well) [26]. The main consequences are the dynamic performance degradation, steady-state errors and the risk of system instability. Therefore, the capability in providing dynamic ancillary services, such as inertial contribution or fault current generation, is affected as well. Indeed, a larger amount of current is needed when providing grid transient support. Moreover, an additive fluctuating power flow can affect the charging operation, with subsequent negative impact on the EV batteries lifetime [14], [27]. Consequently, the implementation of decoupling solutions should be considered to limit the current injection and avoid interference with the charging process.

To solve the coupling issue, many power decoupling solutions are available in the literature for power converters with grid-forming capabilities, such as VSM-embedded grid-tied inverters [28], [29], [30], [31], [32], [33], [34], [35], [36], [37], [38], [39], [40], [41]. The virtual impedance method [28], [29], [30], [31] is one of the most adopted solution available in the literature. However, its decoupling capability is limited, as demonstrated in [30]. Furthermore, this method only addresses the coupling due to the line resistance, while the small load angle assumption error is not considered [26]. Moreover, such solution guarantees the decoupling only at steady-state, as also happens for the virtual power [31], [32] and feedforward-based algorithms [33], [34], [35]. More recent papers discussed the dynamic power coupling in VSM controls [36], [37], [38], [39], [40], [41]. The VSM model proposed in [36] aims to reduce the impact of reactive power variations on the active power control, while the reverse coupling is not investigated. Moreover, a partial compensation is achieved, since the line is assumed purely inductive and only the large load angle deviation is counterbalanced. Instead, in [37], the excitation control loop is embedded with a point of common coupling voltage estimator to compensate for the line voltage drop and make reactive power immune to active power loop. Other recent publications have embedded feedforward terms in VSMs active loop [38], [39] to improve the VSM dynamic response. Nevertheless, these methods mainly deal with power reference tracking performance and oscillation suppression, with the power coupling phenomena discussed in the background. A VSM model with simplified virtual steady-state impedance combined with a current reference modification is proposed in [40] to limit the power coupling. While ensuring both active and reactive power decoupling, this solution is designed for a specific VSM model, where the virtual admittance is algebraically implemented. An enhanced feedforward-based method is presented in [41], where a full active–reactive decoupling is achieved and the immunity to grid impedance deviation is guaranteed by a power coupling observer. However, the inaccurate load angle estimation reduces the algorithm performance. Furthermore, all the above methods face the power coupling issues with the goal of improving the dynamic response and the power converters stability, without evaluating the effects on the ancillary services, such as inertial support or fault current injection.

Motivated by the absence of discussion about this topic in the literature, this article proposes a straightforward decoupling solution, based on the implementation of feedforward terms in the VSM model employed for the AFE unit of bidirectional chargers. Such solution guarantees the complete active–reactive power dynamic decoupling while providing grid support, with the following advantages.

1) Feedforward terms are embedded in the VSM excitation control loop to limit the reactive power injection during grid frequency deviations. Therefore, the current stress on the AFE for the inertial support is minimized and a larger amount of the rated current can be allocated to the EV recharging operation.
2) The addition of decoupling terms in the VSM swing equation cancels the active power fluctuations, that can propagate from the ac side to the dc stage in case of grid support during faults, thus affecting the charging process and reducing the EV battery lifetime.

Furthermore, the designed algorithm ensures a full-decoupled dynamic response in case of power references variation while EVs are recharging. The proposed method has been integrated in the VSM model presented in [42]. This method has a high degree of generality, as it can be implemented in any VSM with excitation control loop and mechanical emulation block [15], [16]. This article is an extension of [43], where the effectiveness of the solution was demonstrated in limiting the reactive current during inertial support. In particular, the following new contributions have been added.

1) Analytical description of the VSM linearized electrical model used to derive the feedforward terms of the proposed power decoupling solution.
2) Sensitivity analysis of the algorithm to the grid impedance estimation.
3) Further experimental tests to validate the solution during voltage dips/swells and in case of P–Q references variations.

The rest of this article is organized as follows. Section II provides the VSM model with the description of its functional blocks. Then, the linearized electrical model used to investigate the P–Q coupling issue in VSMs is obtained in Section III. Furthermore, the feedforward terms to be embedded in VSM active–reactive loops are derived and the operation of the proposed decoupling method is explained. Next, the sensitivity of the algorithm to the grid parameters is analyzed in Section IV. Section V is dedicated to the experimental results and the validation of the method in performing the decoupling during inertial support and grid faults. Moreover, the power coupling suppression during EV charging transients is investigated. Finally, Section VI concludes this article.

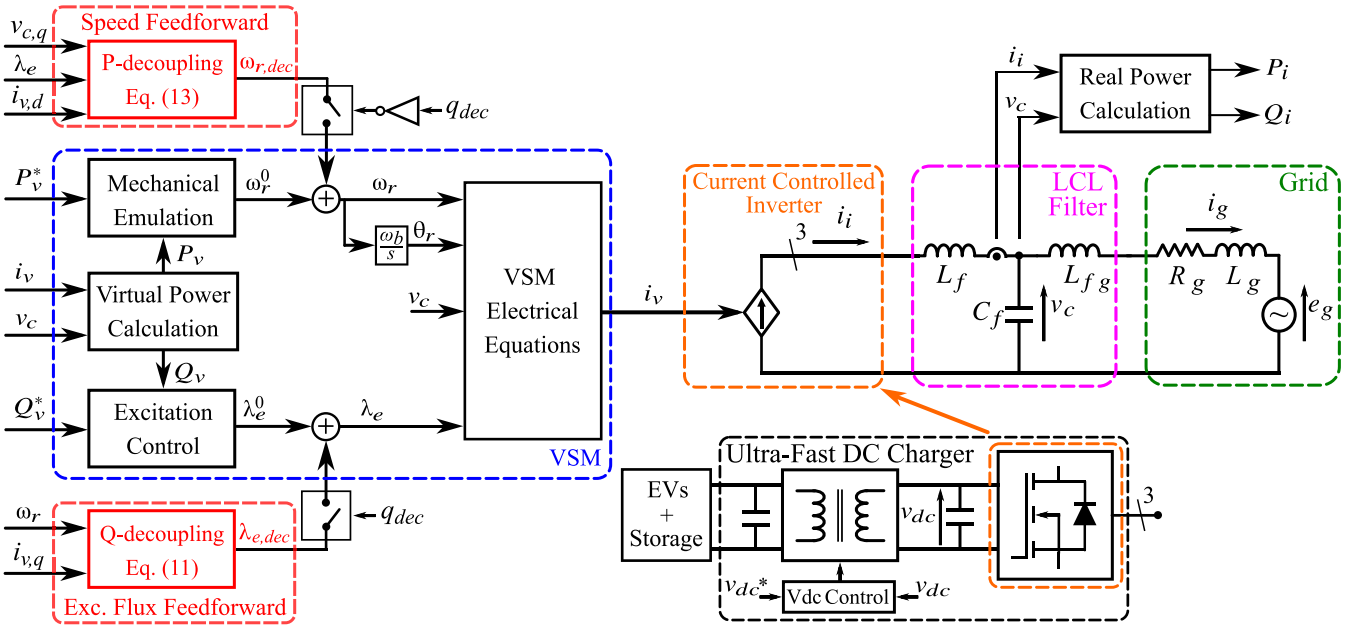

FIGURE 2. Control scheme of the VSM with the proposed feedforward power decoupling method (marked in red). The VSM algorithm provides the references to the AFE current control, while the dc/dcs regulate the dc bus voltage and the power flow between the mains, EV batteries and local storage.

II. VSM MODEL

The considered ultra-fast dc charging system is described in the block diagram of Fig. 2. The ac/dc stage is a VSM driven, current-controlled inverter connected to the grid through an *LCL* filter. The VSM provides the current references to the AFE controller, thus injecting the desired active and reactive powers P_v–Q_v into the mains. Meanwhile, the desired power flow between the grid, EV batteries and local storage is managed by the dc/dcs control, which also performs the dc bus voltage v_{dc} regulation. The VSM model consists of the following functional blocks.

1) *Virtual Power Calculation:* This block computes the VSM virtual powers P_v and Q_v by multiplying the virtual current i_v and the measured voltage v_c across the filter capacitor C_f.
2) *Mechanical Emulation:* It emulates the mechanical behavior of the VSM, by embedding the swing equation of the conventional SGs [25].

$$P_v^* - P_v = 2H\frac{d\omega_r^0}{dt} \tag{1}$$

where P_v^* is the active power reference, H is the inertia constant and ω_r^0 is the virtual rotor speed. Furthermore, any of the damping solutions in the literature must be integrated into the block to suppress the low frequency oscillations [44].
3) *Excitation Control:* This function receives as inputs the reactive power reference Q_v^* and the virtual reactive power Q_v. The virtual excitation flux λ_e^0 is then regulated to provide the desired reactive power exchange with the grid. Different design options are available in the literature for this block, such as the excitation winding model of a real SG, a simple droop-based proportional gain regulator, a purely integral or proportional-integral controller [45].
4) *Electrical Equations:* The resistive and inductive behavior of the VSM stator are emulated through the implementation of a virtual resistance R_v and inductance L_v. The model inputs are v_c, the resulting virtual rotor speed ω_r and excitation flux λ_e and the virtual rotor position θ_r.
5) *P–Q Decoupling Blocks:* The P-decoupling and Q-decoupling blocks are the proposed additive functions to be embedded into the original VSM model, thus performing the power decoupling feature. Indeed, these blocks compute the feedforward terms $\omega_{r,\mathrm{dec}}$-$\lambda_{e,\mathrm{dec}}$ to be added, respectively, to the virtual rotor speed ω_r^0 and excitation flux λ_e^0. The two algorithms are alternately enabled/disabled by the external command q_{dec}. An exhaustive explanation of the two blocks will be provided in Section III.

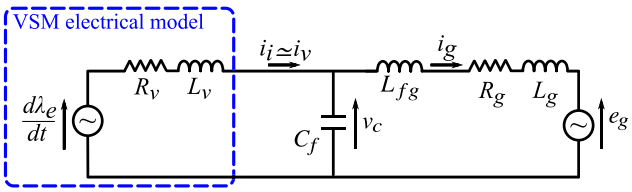

FIGURE 3. Single phase electrical circuit of VSM interfaced to the grid.

The single phase equivalent circuit of the VSM interfacing the mains is reported in Fig. 3. The internal current controller is considered as ideal, with a unity gain transfer function,

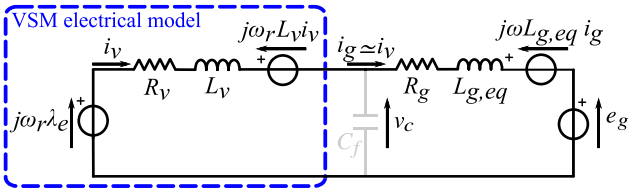

FIGURE 4. Steady state equivalent circuit in the (d,q) reference frame rotating at ω_r. C_f is neglected and an equivalent $L_{g,eq} = L_g + L_{fg}$ is considered.

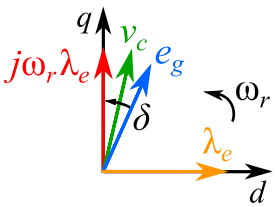

FIGURE 5. Vector diagram of the VSM excitation flux λ_e, the VSM electromotive force $j\omega_r\lambda_e$, the measured voltage v_c and grid voltage e_g in the adopted (d,q) reference frame rotating at ω_r. δ is the load angle.

since its response is several order of magnitude faster than the VSM. Therefore, the inverter output current i_i is considered equal to the reference i_v in the discussion, as well as the inverter output powers P_i and Q_i can be assumed equal to the virtual powers P_v and Q_v. The proposed VSM does not embed active–reactive droop controllers. However, this model can be enabled to perform primary frequency and voltage regulation by implementing two external proportional regulators, thus generating the droop references P_d^* and Q_d^* to be added to P_v^* and Q_v^* [46]

$$P_d^* = \frac{\omega_r^* - \omega_r}{b_p} \tag{2}$$

$$Q_d^* = \frac{\hat{V}_c^* - \hat{V}_c}{b_q} \tag{3}$$

where ω_r^* and $\hat{V}_c^*$ are the grid speed and voltage amplitude references, respectively, b_p and b_q are the droop coefficients.

III. PROPOSED DECOUPLING ALGORITHM

The steady-state equivalent circuit in the (d,q) reference frame rotating at ω_r is obtained by neglecting the current and flux derivative terms (see Fig. 4). λ_e is aligned to the d-axis in the proposed model (see Fig. 5) and the VSM is considered operating under the nominal conditions, with $\omega_r \simeq \lambda_e \simeq 1$ pu. The grid inductance L_g and the grid-side LCL filter inductance L_{fg} can be collected in the equivalent series inductance $L_{g,\text{eq}}$. The steady-state VSM and grid electrical equations in the (d,q) reference frame are (4)–(7)

$$v_{c,d} = \omega_r L_v i_{v,q} - R_v i_{v,d} \tag{4}$$

$$v_{c,q} = \omega_r \lambda_e - \omega_r L_v i_{v,d} - R_v i_{v,q} \tag{5}$$

$$e_{g,d} = \omega_r L_{g,\text{eq}} i_{g,q} - R_g i_{g,d} + v_{c,d} \tag{6}$$

$$e_{g,q} = -\omega_r L_{g,\text{eq}} i_{g,d} - R_g i_{g,q} + v_{c,q} \tag{7}$$

where e_g is the grid voltage and R_g is the grid resistance, which also includes the inherent resistance of the LCL filter grid-side inductor.

The grid current i_g can be considered equal to i_v by neglecting the LCL filter capacitance C_f [47]. Therefore, the resulting equivalent electrical equation in q-axis is obtained combining (5) and (7):

$$e_{g,q} = \omega_r \lambda_e - \omega_r L_{\text{tot}} i_{v,d} - R_{\text{tot}} i_{v,q} \tag{8}$$

where the system total inductance L_{tot} is the sum of L_v and $L_{g,\text{eq}}$, as the total resistance R_{tot} is the sum of R_v and R_g.

A. EXCITATION FLUX FEEDFORWARD

The q-axis electrical model described in (8) is linearized around the system operating point as

$$\Delta e_g \cos\delta - e_g \sin\delta \Delta\delta = \Delta\omega_r \lambda_e + \Delta\lambda_e \omega_r - \Delta\omega_r L_{\text{tot}} i_{v,d} - \omega_r L_{\text{tot}} \Delta i_{v,d} - R_{\text{tot}} \Delta i_{v,q} \tag{9}$$

where e_g is the grid voltage amplitude and δ is the load angle. In case of small speed variations around the operating point with low reactive current injection into the grid, $\Delta\omega_r L_{\text{tot}} i_{v,d}$ is negligible. The term $\sin\delta\Delta\delta$ depends both on load angle ($\sin\delta$) and its deviation ($\Delta\delta$), thus resulting much smaller than the other terms related to ω_r and λ_e. In case of stable grid voltage amplitude ($\Delta e_g \simeq 0$), the q-axis linearized equation is simplified as

$$\Delta\omega_r \lambda_e + \Delta\lambda_e \omega_r - \omega_r L_{\text{tot}} \Delta i_{v,d} - R_{\text{tot}} \Delta i_{v,q} = 0 \tag{10}$$

The link between the virtual speed, the excitation flux and the VSM currents variations is thus demonstrated. Moreover, the role of the virtual and real impedance is highlighted in the power coupling issue.

Since λ_e is aligned with the d-axis, v_c is mainly oriented on the q-axis (see Fig. 5). Therefore, the active power depends on the $i_{v,q}$ current component (i.e., $P_v \approx v_{c,q} \cdot i_{v,q}$) and the reactive power on $i_{v,d}$ (i.e., $Q_v \approx v_{c,q} \cdot i_{v,d}$). In case of P_v-$i_{v,q}$ variation during inertial support, undesired Q_v-$i_{v,d}$ are injected into the grid according to (10). However, a feedforward term $\lambda_{e,\text{dec}}$ can be added to the excitation flux, thus limiting the $i_{v,d}$ deviation and consequently the reactive power injection. The feedforward term is derived from (10) by forcing $\Delta i_{v,d} \simeq 0$ and considering $\omega_r \simeq \lambda_e \simeq 1$ pu.

$$\lambda_{e,\text{dec}} = -\Delta\omega_r + R_{\text{tot}} \Delta i_{v,q}. \tag{11}$$

The term $\lambda_{e,\text{dec}}$ compensates for the power coupling due to the total system resistance, the speed variation, consequently, to the load angle transient deviation.

B. SPEED FEEDFORWARD

Similarly to the previous section, the Q_v–$i_{v,d}$ injection in case of grid support during faults generates undesired P_v–$i_{v,q}$ variations. However, e_g widely changes with voltage dips or swells. Therefore, the main assumptions of (10) are no longer valid and the relation cannot be used to compute a P-decoupling

term. Nevertheless, an equivalent speed feedforward can be obtained by linearizing and simplifying the q-axis VSM electrical (5)

$$\Delta v_{c,q} = \Delta\omega_r \lambda_e + \Delta\lambda_e \omega_r - \omega_r L_v \Delta i_{v,d} - R_v \Delta i_{v,q}. \quad (12)$$

The decoupling term is obtained by forcing $\Delta i_{v,q} \simeq 0$ and considering $\omega_r \simeq \lambda_e \simeq 1$ pu.

$$\omega_{r,\text{dec}} = \Delta v_{c,q} - \Delta\lambda_e + L_v \Delta i_{v,d} \quad (13)$$

where $\Delta v_{c,q}$ compensates for the grid voltage variation, while the other terms limit the P–Q coupling inside the VSM.

C. DECOUPLING FEATURE SELECTION

Both $\omega_{r,\text{dec}}$ and $\lambda_{e,\text{dec}}$ compensate for the P–Q coupling by limiting the mutual $i_{v,d} - i_{v,q}$ coupling and their dependence on virtual speed, excitation flux, and grid voltage on the q-axis. Therefore, the two decoupling algorithms cannot be enabled simultaneously without interfering with each other and leading to VSM instability. The desired decoupling feature is selected through the external command q_{dec}.

1) *Q-decoupling:* It is enabled by setting $q_{\text{dec}} = 1$. It limits the Q_v deviation during active power transients, such as the provision of inertial support, or variations in the EVs power charging request. An extra term $\lambda_{e,\text{dec}}$ is added to the excitation flux λ_e^0 obtained from the reactive controller;
2) *P-decoupling:* It is enabled when $q_{\text{dec}} = 0$. It almost cancels the P_v fluctuations in case of reactive power transients, i.e., when a grid fault occurs, or in case of Q_v^* variations. The feedforward $\omega_{r,\text{dec}}$ is added to the ω_r^0, which is computed with (1).

A full explanation regarding the implementation of the proposed decoupling algorithm is provided in the Appendix.

IV. SENSITIVITY TO GRID IMPEDANCE ESTIMATION

While the P-decoupling feedforward $\omega_{r,\text{dec}}$ is not affected by the grid impedance, the Q-decoupling term $\lambda_{e,\text{dec}}$ depends on the correct estimation of the grid resistance R_g. Therefore, a proper online R_g computation is needed to obtain the full compensation of the reactive power coupling. To this purpose, several techniques are available in the literature to perform the grid impedance estimation, thus real-time updating the Q-decoupling algorithm [48]. The excess reactive current $\Delta i_{v,d,\text{err}}$ due to the incorrect R_g estimation can be derived from (10) and it is expressed as follows:

$$\Delta i_{v,d,\text{err}} = \frac{R_{g,\text{est}} - R_g}{L_v + L_{g,\text{eq}}} \Delta i_{v,q} \quad (14)$$

where $R_{g,\text{est}}$ is the estimated grid resistance.

This undesired current depends on the grid parameters, the grid resistance estimation error, the VSM inductance and the amount of active current $\Delta i_{v,q}$. Since $P_v \approx v_{c,q} \cdot i_{v,q}$ and $Q_v \approx v_{c,q} \cdot i_{v,d}$, the ratio between the extra reactive power $\Delta Q_{v,\text{err}}$ and the active power variation ΔP_v can be derived from (14) and expressed as a function of the short circuit ratio (SCR), the X/R ratio, the virtual inductance L_v and the relative

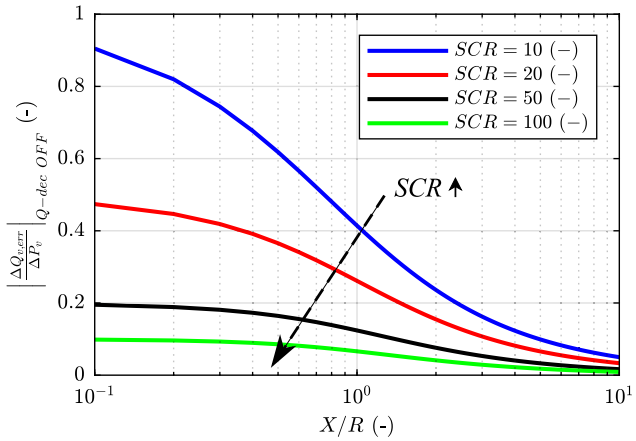

FIGURE 6. Extra reactive power $\Delta Q_{v,\text{err}}$ injected into the grid when an active power variation ΔP_v occurs and Q-decoupling algorithm is not performed. The *x*-axis is in logarithmic scale.

estimation error $\epsilon_{R_g} = (R_{g,\text{est}} - R_g)/R_g$

$$\frac{\Delta Q_{v,\text{err}}}{\Delta P_v} = \frac{\epsilon_{R_g}}{(\frac{X}{R}) + L_v \cdot \text{SCR}\sqrt{1 + (\frac{X}{R})^2}}. \quad (15)$$

The uncompensated reactive power is proportional to ΔP_v, linear dependent on ϵ_{R_g}, while it reduces if the VSM is interfaced to a low impedance grid (high SCR) with prevailing inductive behavior (high X/R). Consequently, particular care must be taken in case of ultra-weak and resistive grids.

When an active power variation occurs and the Q-decoupling is not enabled, the amount of drawn reactive power can be computed by (15), by setting $R_{g,\text{est}} = 0$ and consequently, $\epsilon_{R_g} = -1$

$$\left|\frac{\Delta Q_{v,\text{err}}}{\Delta P_v}\right|_{Q-\text{dec OFF}} = \frac{1}{(\frac{X}{R}) + L_v \cdot \text{SCR}\sqrt{1 + (\frac{X}{R})^2}}. \quad (16)$$

The variation of $|\Delta Q_{v,\text{err}}/\Delta P_v|_{Q-\text{dec OFF}}$, as a function of the X/R ratio for different SCR, is shown in Fig. 6. The VSM inductance L_v is defined by the user and is set to a typical value of 0.1 pu. In case of a weak and prevailing resistive grid with SCR = 10 and $X/R = 0.1$, the amount of undesired reactive power due to the coupling issue is almost equal to the active power variation, with $\Delta Q_{v,\text{err}} = -0.9 \cdot \Delta P_v$. Meanwhile, the power coupling effect is negligible when SCR is higher than 100 or X/R is higher than 10.

V. EXPERIMENTAL RESULTS

The proposed feedforward decoupling algorithm has been experimentally validated on a 15 kVA two-level three-phase inverter controlled by a dSPACE 1005 platform with 10 kHz of switching f_{sw} and sampling f_s frequencies. The system configuration used for tests is outlined in the block diagram of Fig. 7, while a picture of the experimental setup is presented in Fig. 8. The inverter is connected through an *LCL* filter to a 50 kVA grid emulator able to provide a 50 Hz 120 V $_{\text{rms}}$

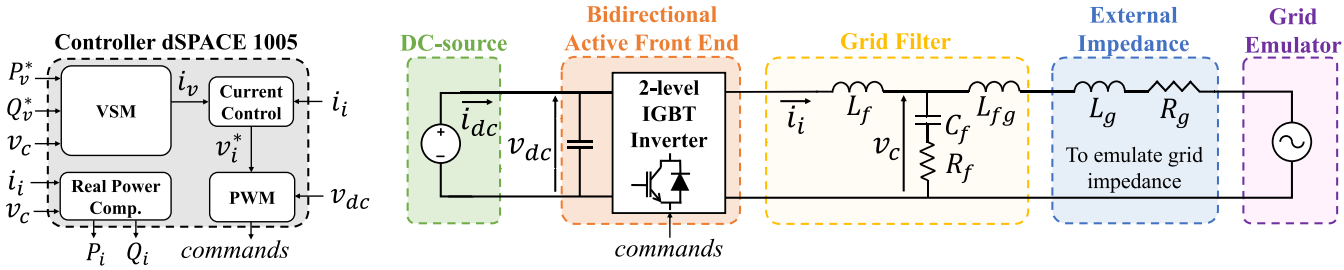

FIGURE 7. Scheme of the system configuration used for tests.

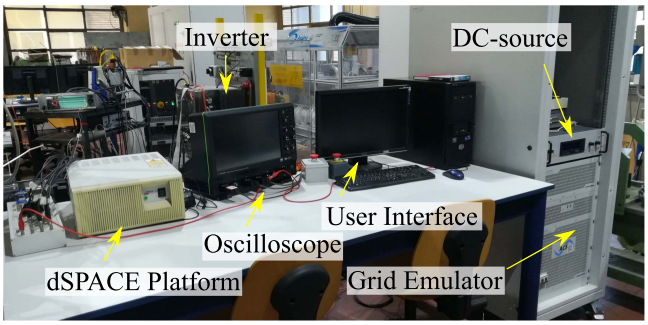

FIGURE 8. Picture of the experimental setup.

TABLE 1. Main Data of the Experimental Setup

Base Values		Inverter		VSM		LCL Filter & Grid	
S_b	15 kVA	S_n	15 kVA	L_v	0.1 pu	L_f	0.059 pu
V_b	170 V	I_n	59 A	R_v	0.02 pu	C_f	0.020 pu
f_b	50 Hz	V_{dc}	380 V	H	4 s	L_{fg}	0.013 pu
Z_b	2.9 Ω	f_{sw}	10 kHz	τ_e	0.1-1 s	L_g	0.033 pu
L_b	9.2 mH	f_s	10 kHz			R_g	0.124 pu
C_b	1.1 mF						

phase voltage. A constant dc-source supplies the dc stage and emulates the local storage and the EV batteries connected to an ultra-fast charging system. A three-phase inductor and a three-phase resistor are placed between the power converter and the grid emulator as grid impedance. The grid equivalent inductance is $L_{g,\text{eq}} = L_{fg} + L_g = 0.046$ p· u·, the *SCR* is 7.58 and X/R is 0.37. The VSM damping solution proposed in [49] is adopted to suppress the VSM speed oscillations. Meanwhile, the excitation control is implemented as in [42]. Therefore, the reactive power control behaves as a first order system with a tunable excitation time constant τ_e. The inverter nominal data, the *LCL* filter and grid parameters, as well as the VSM parameters are reported in Table 1.

Five following experimental tests are performed to experimentally validate the proposed decoupling method.

1) *Test 1:* The VSM inertial response is evaluated during the charging process. The inverter is absorbing an active power $P_i = P_v^* = -0.25$ pu from the grid to store energy into the dc-source when a triangular frequency variation in the range 49.5–50.5 Hz with a period of 2 s is imposed by the grid emulator. The inverter should provide an extra active power according to the VSM tuning and the frequency deviation. Instead, the desired inverter reactive power Q_i is null. The effectiveness of the proposed decoupling algorithm to cancel the reactive power injection without affecting the inertial behavior is demonstrated.
2) *Test 2:* A grid frequency drop is imposed by the grid emulator to simulate a major power imbalance during the charging operation ($P_i = P_v^* = -0.5$ pu). Again, the power Q-decoupling performance are analyzed in case of a severe grid perturbation.
3) *Test 3:* A 10 % voltage dip is applied by the grid emulator, while the inverter is in idle mode ($P_v^* = Q_v^* = 0$). A reactive fault current injection is expected. Meanwhile, the P-coupling algorithm limits the power fluctuations, that may propagate at the dc stage, thus causing undesired fast charging/discharging of the EV batteries.
4) *Test 4:* The benefits of the proposed P–Q decoupling solution are evaluated during the VSM normal dynamical operation. The response of the VSM to different reference steps of active-reactive power is investigated with and without enabling the decoupling algorithm.
5) *Test 5:* The sensitivity of the Q-decoupling algorithm to the grid resistance estimation is studied when a step variation in P_v^* is applied and the reactive power loop is disabled. The Q_i steady-state error is shown for different values of relative estimation error ϵ_{R_g}.

A. INERTIAL RESPONSE

A linear variation of the grid frequency is imposed to evaluate the VSM behavior during inertial support. The excitation controller is tuned to provide a slow response ($\tau_e = 1$ s) with the aim of highlighting the benefits of the proposed decoupling solution. The expected active power injection is proportional to the virtual frequency derivative $\Delta f_r/\Delta t$ as follows:

$$\Delta P_{\text{inertial}} = \frac{2H}{f_b} \cdot \frac{\Delta f_r}{\Delta t} = 0.16 \text{ p·u·} \tag{17}$$

This amount of power is added to the charging power (−0.25 pu) that the inverter was already transferring to the

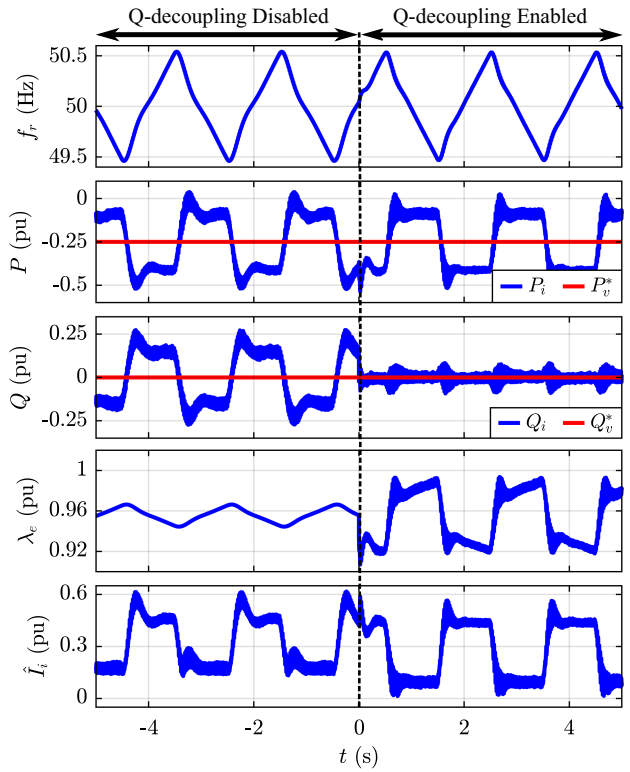

FIGURE 9. Results of Test 1 (inertial behavior). From top to bottom: virtual frequency f_r, inverter active power P_i and virtual active power reference P_v^*, inverter reactive power Q_i and reactive power reference Q_v^*, excitation flux λ_e, output current peak $\hat{I}_i$.

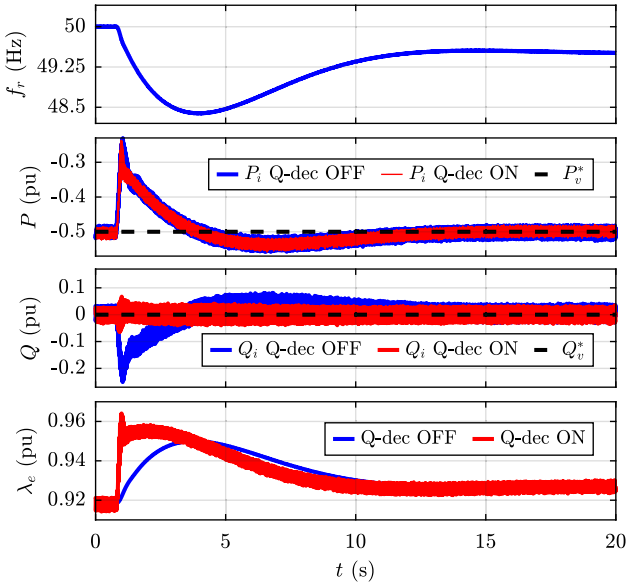

FIGURE 10. Results of Test 2 (inertial behavior). From top to bottom: virtual frequency f_r, inverter active power P_i and virtual active power reference P_v^*, inverter reactive power Q_i and virtual reactive power reference Q_v^*, excitation flux λ_e.

dc-source. In case of field applications in ultra-fast dc charging systems, $\Delta P_{\text{inertial}}$ is provided or absorbed by the locally installed off-board storage, or directly by the EV batteries, according to the ultra-fast charger hardware configuration (see Fig. 1). Initially, the power decoupling is not performed and a maximum reactive power of 0.25 pu is provided. As shown in Fig. 9, at time $t = 0$ s, the Q-decoupling algorithm is enabled and the reactive power is almost canceled without affecting the active power injection. Indeed, the Q-decoupling algorithm provides the $\Delta\lambda_e = \lambda_{e,\text{dec}}$ needed to instantaneously compensate for the reactive coupling issue. Furthermore, the peak of the current injected into the grid is reduced by 9.8% (0.61 pu vs. 0.55 pu). Therefore, a larger current capability is available for the charging operation, when the AFE is performing grid support.

B. GRID FREQUENCY DROP

In Test 2 (see Fig. 10) a severe grid frequency drop due to a large power imbalance is emulated. This curve profile can be obtained in case of a major generator disconnection from the mains. The grid frequency drops to a nadir of 48.39 Hz and then settles to a final value of 49.50 Hz. Meanwhile, the inverter is providing 0.5 pu of active power to the dc-source. The imposed frequency variation is deliberately severe, with low nadir, high initial derivative and low frequency after fault, to highlight the effectiveness of the Q-decoupling algorithm. The test is performed with and without the proposed feedforward decoupling. The reactive controller is tuned to achieve $\tau_e = 1$ s in both cases. The obtained results confirm the outcomes of Test 1. Indeed, the proposed decoupling method does not affect the inertial behavior, while limiting the reactive power and the injected current to perform the inertial support.

C. VOLTAGE DIP

A voltage dip of 10% is applied to evaluate the P-decoupling algorithm performance in case of a short circuit in the mains (see Fig. 11). The fault condition occurs when the inverter is not providing active and reactive power ($P_v^* = Q_v^* = 0$). Therefore, the power transfer from the dc-source to the grid during the test will be exclusively due to power coupling issue. The excitation time constant τ_e is reduced to 0.1s, thus speeding up the reactive control response. At $t = 0$ s, the voltage dip occurs. If the P-decoupling algorithm is not enabled, an undesired amount of active power is injected into the grid, with a peak value of 0.32 pu. Furthermore, the power fluctuations propagate through the inverter to the dc side. Indeed, a non negligible fluctuating current i_{dc} is absorbed from the dc stage. This fast peak current would be drawn in first instance from the dc-link capacitors, according to their energy capability. Then, without an installed local storage, this current would be absorbed from the EVs connected to the charging system, with possible negative consequences on the batteries lifetime. Instead, when the P-decoupling algorithm is activated, the active power injection into the grid is almost canceled.

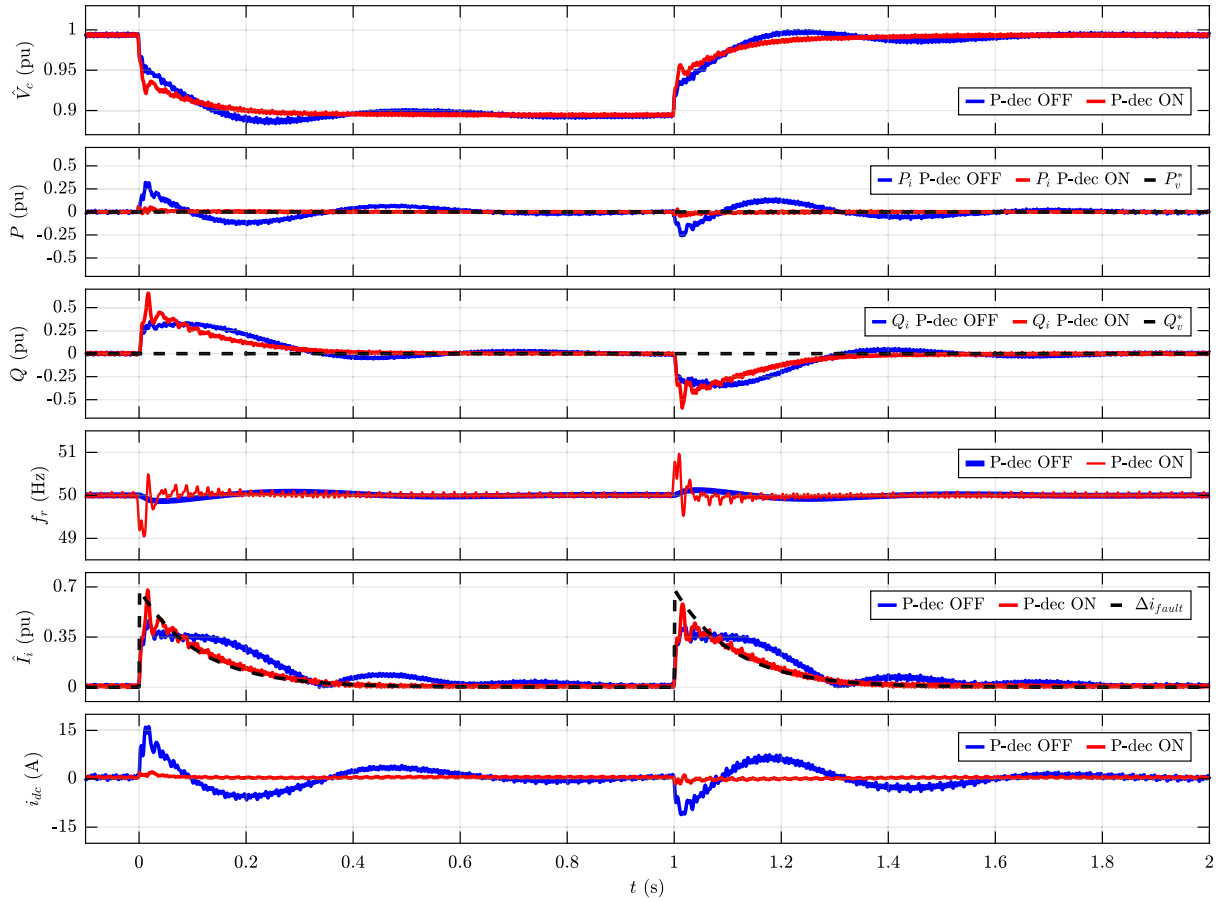

FIGURE 11. Results of Test 3 (voltage dip) without and with the P-decoupling algorithm enabled. From top to bottom: grid measured voltage peak $\hat{V}_c$, virtual active power P_v and active power reference P_v^*, reactive power Q_v and reactive power reference Q_v^*, virtual frequency f_r, inverter output current peak $\hat{I}_i$, current absorbed from the DC-source i_{dc}.

Meanwhile, the dc side operation is no more influenced by the provision of grid support during faults. Moreover, the desired fault current profile can be easily achieved when the P-decoupling algorithm is enabled. Indeed, the behavior of the fault current Δi_{fault} can be expressed as follows:

$$\Delta i_{\text{fault}} = \frac{\Delta V_{\text{dip}}}{L_v + L_{g,\text{eq}}} \cdot e^{-t/\tau_e} \tag{18}$$

where ΔV_{dip} is the voltage dip amplitude during the fault condition (0.1 pu in the proposed test).

Therefore, the VSM inductance and the excitation controller time constant can be tuned to satisfy the needed support requirements in case of faults. The current injection amplitude is regulated by L_v, while the duration of the event by τ_e. At $t = 1$ s, the grid voltage returns to nominal condition (1 pu) and again the benefits of the proposed P-decoupling algorithms are observed. Indeed, the active power and dc current fluctuations are almost eliminated.

D. DYNAMICAL OPERATION

The dynamical performance of the VSM embedded with the proposed decoupling solution is verified by assessing the response to different steps of active and reactive power references (see Fig. 12). The desired decoupling algorithm is enabled according to the power reference variation. In detail, the P-decoupling algorithm is enabled by setting $q_{\text{dec}} = 0$ before a Q_v^* change. Instead, the Q-decoupling algorithm is activated by setting $q_{\text{dec}} = 1$ before a P_v^* variation. When a decoupling algorithm is activated, the other one is automatically excluded to avoid interference. The excitation flux time constant τ_e is set to 0.1 s to achieve a similar response time for the VSM active and reactive control loops. Initially, the inverter operates with zero power references (i.e., $P_v^* = Q_v^* = 0$). Then, a P_v^* step variation of 0.5 pu is requested at $t = 0$ s. After 1s, also the reactive power reference is step-changed to -0.5 pu. Finally, active and reactive power inversions are performed, respectively, at $t = 2$ s and $t = 3$ s. Even in case of stressful test conditions, such as step power inversions, the proposed P-decoupling and Q-decoupling algorithms fully compensate for the power coupling issues, both in case of P_v^* and Q_v^* changes. Indeed, the Q_i fluctuations are suppressed when P_i deviates and vice versa. Moreover, the power responses become more damped, while maintaining the same rise time.

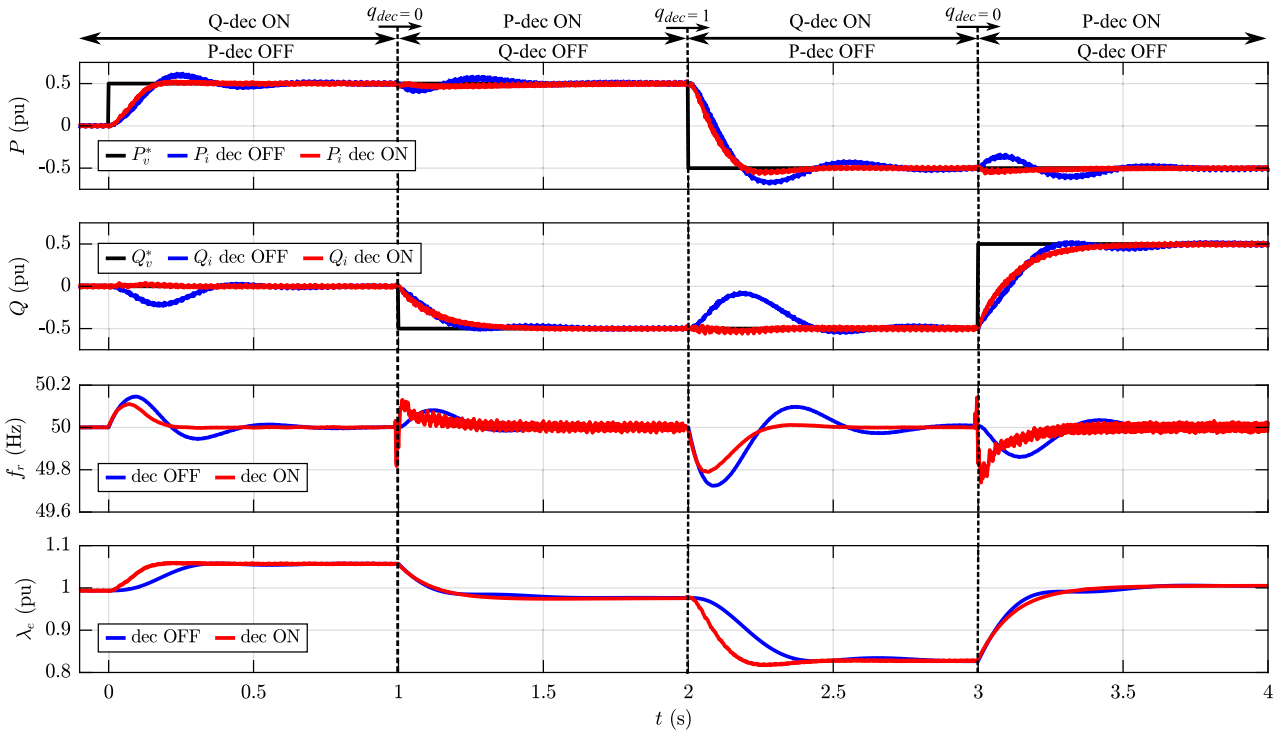

FIGURE 12. Results of Test 4 (dynamic performance). From top to bottom: inverter active power P_i and virtual active power reference P_v^*, inverter reactive power Q_i and virtual reactive power reference Q_v^*, virtual frequency f_r, excitation flux λ_e.

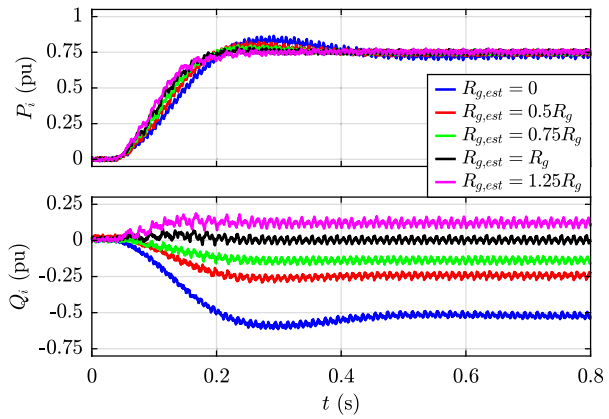

FIGURE 13. Results of Test 5: effect of a wrong grid resistance estimation. From top to bottom: inverter active power P_i, inverter reactive power Q_i.

TABLE 2. Comparison of the Results of Test 5 With the Theoretical Values Obtained in Section IV

$R_{g,est}/R_g$ (%)	ε_{R_g} (%)	ΔQ_i (pu)	$\Delta Q_{v,err}$ (pu)
0	-100	-0.52	-0.64
50	-50	-0.24	-0.32
75	-25	-0.14	-0.16
100	+0	+0.00	+0.00
125	+25	+0.12	+0.16

E. SENSITIVITY TO GRID RESISTANCE ESTIMATION

The influence of R_g estimation on the Q-decoupling algorithm effectiveness is investigated with this test. The reactive controller is disabled by setting to zero its integral gain. Therefore, the excitation flux variations will be due to the computed feedforward $\lambda_{e,\mathrm{dec}}$. A step of 0.75 pu in the active power is applied and the reactive response is analyzed in case of different values of estimated grid resistance, i.e. $R_{g,\mathrm{est}}$ equal to 0% , 50% , 75% , 100% , and 125% of R_g (see Fig. 13). The ΔQ_i deviations measured at the end of the transient response are then compared with the expected theoretical values $\Delta Q_{v,\mathrm{err}}$ obtained by means of (15). The results are reported in Table 2. It can be observed that the measured values are consistent with the theoretical ones. A larger deviation between measurements and expected values is observed in case of high estimation errors (i.e., $R_{g,\mathrm{est}} = 0$). The difference in results can be explained by the fact that $\Delta Q_{v,\mathrm{err}}$ is obtained by applying small-signal analysis, where a mild variation around an operating point is expected. Instead, in this test, a large variation of active power is imposed ($\Delta P_i = 0.75$ pu). Moreover, in case of inaccurate R_g estimation, the significant Q_i deviation from the initial steady-state condition further affects the gap. However, the outcomes of Test 5 confirm the effectiveness of the proposed Q-decoupling algorithm. Indeed, with a proper R_g estimation, the reactive power injection is canceled ($\Delta Q_i = 0$ pu), even in case of large active power variations.

VI. CONCLUSION

This article proposes a full (active and reactive) power decoupling solution for VSM controls to compensate for power coupling issues in case of fast grid transient events, such as frequency variations or voltage dips and swells. By enabling the Q-decoupling feature, feedforward terms are added to the output of the VSM excitation controller. Therefore, the reactive power injection is canceled when providing inertial support. Instead, by enabling the P-decoupling algorithm, feedforward terms are integrated in the VSM swing equation. Consequently, the active power fluctuations are limited when the AFE injects short circuit current into the grid during faults. Nevertheless, the designed algorithm ensures a full-decoupled dynamic response of the VSM also in case of power references variation.

This method results well suitable for VSMs embedded into the AFE control of ultra-fast dc charging systems. Indeed, in these applications the current effort for the grid support has to be minimized, since the largest possible power capability has to be allocated for the EV charging operation. The feature selection (P-decoupling or Q-decoupling) can be executed by setting the external command q_{dec}. When an active or reactive power reference variation is requested by the user, the required feature can be pre-selected, thus performing the correct power decoupling. Instead, grid perturbations cannot be predicted in advance. Therefore, particular care must be taken in the feature selection when the EV charger is in steady-state. The choice can be based on the agreements with the power system operator regarding which ancillary services have to be provided. Otherwise, the EV charger hardware can be considered.

The Q-decoupling algorithm limits the AFE current stress during inertial support. Therefore, a larger amount of the rated current can be used for the charging process and the AFE has not to be current oversized to emulate the inertial behavior.

The P-decoupling algorithm cancels the ac and dc power fluctuations when the AFE injects reactive current into the grid during voltage dips and swells. Since this power would be absorbed in first instance from the dc-link capacitors, their oversizing in terms of energy is thus prevented.

With installed local storage [see Fig. 1(a)], the mains and EVs are power decoupled by hardware. Indeed, the local storage can take charge of absorbing or providing the requested fluctuating power during grid faults. Instead, in case of ultra-fast charging configurations without local storage [see Fig. 1(b)], these uncontrolled power fluctuations could propagate to EV batteries and cause fast charging/discharging events, resulting in a potential risk for the batteries lifetime.

Therefore, the authors suggest to keep enabled the Q-decoupling algorithm when the dc charger is in steady-state in the presence of installed local storage. Otherwise, the P-decoupling algorithm is preferred. Experimental tests are performed on a 15 kVA two-level three-phase inverter, emulating the AFE of a dc charging infrastructure. The experimental results validate the proposed decoupling method, confirming that VSM controls implemented in ultra-fast charging applications are a promising solution to guarantee the stability of the electric power system.

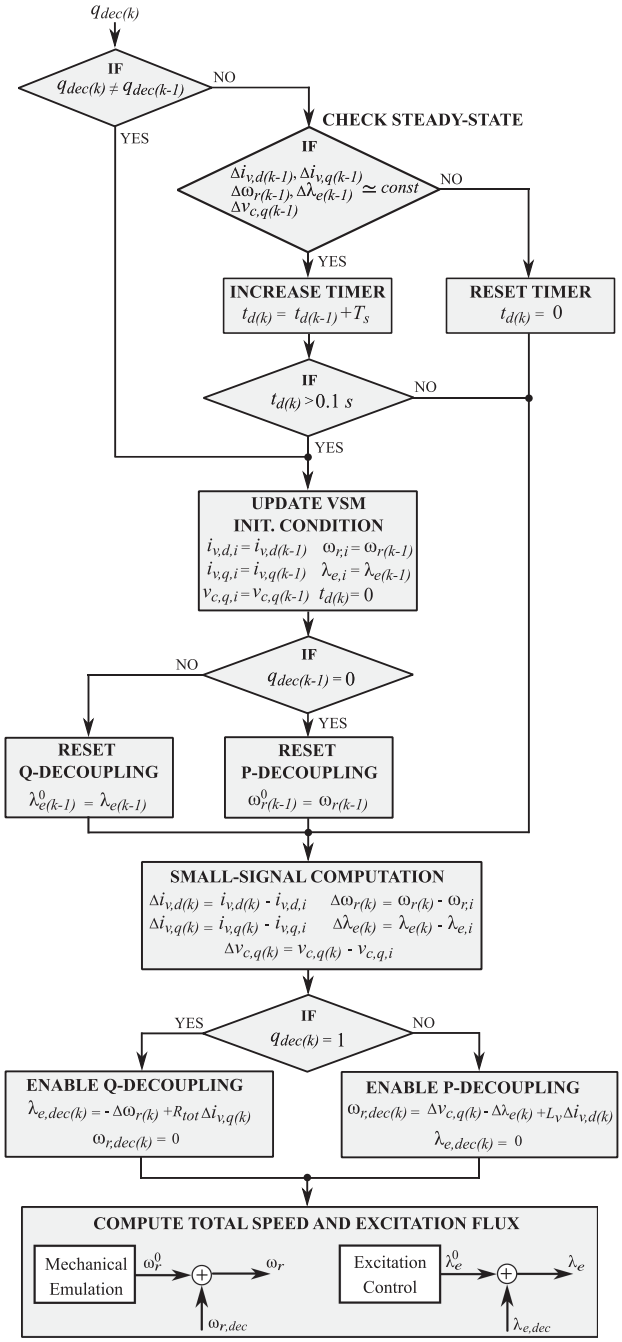

FIGURE 14. Flowchart of the proposed power decoupling algorithm executed at sampling period *k*. T_s is the sampling time.

APPENDIX

The proposed decoupling solution is outlined in the flowchart of Fig. 14. The decoupling feature selection (P-decoupling or Q-decoupling) can be real-time performed every sampling period $T_s = \frac{1}{f_s}$ by modifying q_{dec} and updating the VSM initial

condition values $i_{v,i}$, $v_{c,i}$, $\lambda_{e,i}$, $\omega_{r,i}$, which are used to compute the small-signal deviation terms $\Delta i_{v,d}$, $\Delta i_{v,q}$, $\Delta v_{c,q}$, $\Delta\lambda_e$ and $\Delta\omega_r$. Indeed, $\omega_{r,\text{dec}}$ and $\lambda_{e,\text{dec}}$ will be determined by linearizing the VSM model around the new steady state condition. Furthermore, the values λ_e^0-ω_r^0 are forced equal to λ_e-ω_r when the corresponding decoupling algorithm is disabled, thus integrating the feedforward residuals into the outputs of the VSM electromechanical blocks and ensuring continuity in the excitation flux and virtual speed computation. Furthermore, the system initial values are updated and the decoupling algorithms are reinitialized even if a steady-state condition is observed for a defined period (0.1 s).

REFERENCES

[1] IEA, "Global EV outlook 2024 - Analysis," IEA, Paris, France, Rep., Apr. 2024. [Online]. Available: https://www.iea.org/reports/global-ev-outlook-2024

[2] S. Srdic and S. Lukic, "Toward extreme fast charging: Challenges and opportunities in directly connecting to medium-voltage line," *IEEE Electrific. Mag.*, vol. 7, no. 1, pp. 22–31, Mar. 2019.

[3] S. Mateen, M. Amir, A. Haque, and F. Ilahi Bakhsh, "Ultra-fast charging of electric vehicles: A review of power electronics converter, grid stability and optimal battery consideration in multi-energy systems," *Sustain. Energy Grids Netw.*, vol. 35, 2023, Art. no. 101112.

[4] H. Tu, H. Feng, S. Srdic, and S. Lukic, "Extreme fast charging of electric vehicles: A technology overview," *IEEE Trans. Transport. Electrific.*, vol. 5, no. 4, pp. 861–878, Dec. 2019.

[5] S.-A. Amamra and J. Marco, "Vehicle-to-grid aggregator to support power grid and reduce electric vehicle charging cost," *IEEE Access*, vol. 7, pp. 178528–178538, 2019.

[6] J. Fang, H. Li, Y. Tang, and F. Blaabjerg, "On the inertia of future more-electronics power systems," *IEEE Trans. Emerg. Sel. Topics Power Electron.*, vol. 7, no. 4, pp. 2130–2146, Dec. 2019.

[7] S. Panchanathan et al., "A comprehensive review of the bidirectional converter topologies for the vehicle-to-grid system," *Energies*, vol. 16, no. 5, Mar. 2023, Art. no. 2503. [Online]. Available: https://www.mdpi.com/1996-1073/16/5/2503

[8] "High penetration of power electronic interfaced power sources and the potential contribution of grid forming converters," ENTSO-E, Brussels, Tech. Rep., Jan. 2020. [Online]. Available: https://ieeexplore.ieee.org/abstract/document/10149420https://www.entsoe.eu/events/2020/01/30/workshop-on-high-penetration-of-power-electronic-interfaced-power-sources-and-the-potential-contribution-of-grid-forming-converters/

[9] "Grid-forming capabilities: Towards system level integration," ENTSO-E, Brussels, Mar. 2021. [Online]. Available: https://eepublicdownloads.entsoe.eu/clean-documents/RDC%20documents/210331_Grid%20Forming%20Capabilities.pdf

[10] J. A. Suul, S. D'Arco, and G. Guidi, "Virtual synchronous machine-based control of a single-phase bi-directional battery charger for providing vehicle-to-grid services," *IEEE Trans. Ind. Appl.*, vol. 52, no. 4, pp. 3234–3244, Jul./Aug. 2016.

[11] X. Yan et al., "Virtual synchronous motor based-control of a three-phase electric vehicle off-board charger for providing fast-charging service," *Appl. Sci.*, vol. 8, no. 6, May 2018, Art. no. 856. [Online]. Available: https://www.mdpi.com/2076-3417/8/6/856

[12] J. D. Paucara, J. C. U. Peña, and D. Sal y Rosas, "HESS management for virtual inertia, frequency and voltage support through off-board EV bidirectional chargers," *IEEE Open J. Ind. Electron. Soc.*, vol. 5, pp. 376–385, 2024.

[13] F. Mandrile, D. Cittanti, V. Mallemaci, and R. Bojoi, "Electric vehicle ultra-fast battery chargers: A boost for power system stability?," *World Electric Veh. J.*, vol. 12, no. 1, Art. no. 16, Mar. 2021. [Online]. Available: https://www.mdpi.com/2032-6653/12/1/16

[14] M. Kesler, M. C. Kisacikoglu, and L. M. Tolbert, "Vehicle-to-grid reactive power operation using plug-in electric vehicle bidirectional offboard charger," *IEEE Trans. Ind. Electron.*, vol. 61, no. 12, pp. 6778–6784, Dec. 2014.

[15] M. Shadoul et al., "A comprehensive review on a virtual-synchronous generator: Topologies, control orders and techniques, energy storages, and applications," *Energies*, vol. 15, no. 22, Nov. 2022, Art. no. 8406. [Online]. Available: https://www.mdpi.com/1996-1073/15/22/8406

[16] V. Mallemaci, F. Mandrile, S. Rubino, A. Mazza, E. Carpaneto, and R. Bojoi, "A comprehensive comparison of virtual synchronous generators with focus on virtual inertia and frequency regulation," *Electric Power Syst. Res.*, vol. 201, 2021, Art. no. 107516.

[17] F. Mandrile, F. Stella, E. Carpaneto, and R. Bojoi, "Grid fault current injection using virtual synchronous machines featuring active junction temperature limitation of power devices," *IEEE Trans. Emerg. Sel. Topics Power Electron.*, vol. 10, no. 5, pp. 6243–6251, Oct. 2022.

[18] K. Oureilidis et al., "Ancillary services market design in distribution networks: Review and identification of barriers," *Energies*, vol. 13, no. 4, Feb. 2020, Art. no. 917. [Online]. Available: https://www.mdpi.com/1996-1073/13/4/917

[19] Terna, "Pilot project fast reserve," 2020. [Online]. Available: https://download.terna.it/terna/Fast% 20Reserve%20-%20Information%20pack_8d82fe02cbed7ad.pdf

[20] Fingrid, "Fast frequency reserve," 2020. [Online]. Available: https://www.fingrid.fi/en/electricity-market/reserves_and_balancing/fast-frequency-reserve/

[21] European Parliament, "Directive (EU) 2019/944 of the European parliament and of the council on common rules for the internal market for electricity and amending directive 2012/27/EU," Jun. 2019. [Online]. Available: https://eur-lex.europa.eu/legal-content/EN/TXT/PDF/?uri=CELEX:32019L0944

[22] European Commission, "What is an energy community? Rural Energy Community Hub," 2024. [Online]. Available: https://wayback.archive-it.org/12090/20240320084824/https://rural-energy-community-hub.ec.europa.eu/index_en

[23] M. Delfanti, A. Galliani, and V. Olivieri, "The new role of DSOs: Ancillary services from res towards a local dispatch," 2014. [Online]. Available: https://www.semanticscholar.org/paper/THE-NEW-ROLE-OF-DSOs%3A-ANCILLARY-SERVICES-FROM-RES-A-Delfanti-Galliani/1dfc087480fc707ca1dc16f802738a97ab989ea3

[24] S. Granata, M. Di Benedetto, C. Terlizzi, R. Leuzzi, S. Bifaretti, and P. Zanchetta, "Power electronics converters for the internet of energy: A review," *Energies*, vol. 15, no. 7, Apr. 2022, Art. no. 2604. [Online]. Available: https://www.mdpi.com/1996-1073/15/7/2604

[25] P. Kundur, *Power System Stability and Control*. New York, NY, USA: McGraw-Hill Education, Jan. 1994.

[26] M. Li et al., "Unified modeling and analysis of dynamic power coupling for grid-forming converters," *IEEE Trans. Power Electron.*, vol. 37, no. 2, pp. 2321–2337, Feb. 2022.

[27] K. Uddin, A. D. Moore, A. Barai, and J. Marco, "The effects of high frequency current ripple on electric vehicle battery performance," *Appl. Energy*, vol. 178, pp. 142–154, 2016.

[28] J. M. Guerrero, L. G. de Vicuna, J. Matas, M. Castilla, and J. Miret, "Output impedance design of parallel-connected ups inverters with wireless load-sharing control," *IEEE Trans. Ind. Electron.*, vol. 52, no. 4, pp. 1126–1135, Aug. 2005.

[29] H. Mahmood, D. Michaelson, and J. Jiang, "Accurate reactive power sharing in an islanded microgrid using adaptive virtual impedances," *IEEE Trans. Power Electron.*, vol. 30, no. 3, pp. 1605–1617, Mar. 2015.

[30] T. Wen, D. Zhu, X. Zou, B. Jiang, L. Peng, and Y. Kang, "Power coupling mechanism analysis and improved decoupling control for virtual synchronous generator," *IEEE Trans. Power Electron.*, vol. 36, no. 3, pp. 3028–3041, Mar. 2021.

[31] J. Rocabert, A. Luna, F. Blaabjerg, and P. Rodríguez, "Control of power converters in AC microgrids," *IEEE Trans. Power Electron.*, vol. 27, no. 11, pp. 4734–4749, Nov. 2012.

[32] T. Wu, Z. Liu, J. Liu, S. Wang, and Z. You, "A unified virtual power decoupling method for droop-controlled parallel inverters in microgrids," *IEEE Trans. Power Electron.*, vol. 31, no. 8, pp. 5587–5603, Aug. 2016.

[33] X. Yan and Y. Zhang, "Power coupling analysis of inverters based on relative gain method and decoupling control based on feedforward compensation," in *Proc. Int. Conf. Renewable Power Gener.*, 2015, pp. 1–5.

[34] M. Li et al., "A power decoupling control strategy for droop controlled inverters and virtual synchronous generators," in *Proc. IEEE 8th Int. Power Electron. Motion Control Conf. (IPEMC-ECCE Asia)*, 2016, pp. 1713–1719.

[35] T. Wen, X. Zou, X. Guo, D. Zhu, L. Peng, and X. Wang, "Feedforward compensation control for virtual synchronous generator to improve power decoupling capability," in *Proc. 14th IEEE Conf. Ind. Electron. Appl. (ICIEA)*, 2019, pp. 2528–2533.
[36] S. Dong and Y. Christine Chen, "Reducing transient active- and reactive-power coupling in virtual synchronous generators," in *Proc. IEEE 28th Int. Symp. Ind. Electron.*, 2019, pp. 1090–1095.
[37] B. Li, L. Zhou, X. Yu, C. Zheng, and J. Liu, "Improved power decoupling control strategy based on virtual synchronous generator," *IET Power Electron.*, vol. 10, no. 4, pp. 462–470, 2017.
[38] M. Li, Y. Wang, Y. Liu, N. Xu, S. Shu, and W. Lei, "Enhanced power decoupling strategy for virtual synchronous generator," *IEEE Access*, vol. 8, pp. 73601–73613, 2020.
[39] S. D'Arco and J. A. Suul, "Phase angle feed-forward control for improving the power reference tracking of virtual synchronous machines," *IEEE Trans. Ind. Appl.*, vol. 60, no. 1, pp. 851–864, Jan./Feb. 2024.
[40] A. Liu, J. Liu, and Q. Wu, "Improvement of VSG transient performance based on power feedforward decoupling control," *IET Gener. Transmiss. Distrib.*, vol. 16, no. 20, pp. 4080–4095, 2022.
[41] N. Dong, M. Li, X. Chang, W. Zhang, H. Yang, and R. Zhao, "Robust power decoupling based on feedforward decoupling and extended state observers for virtual synchronous generator in weak grid," *IEEE Trans. Emerg. Sel. Topics Power Electron.*, vol. 11, no. 1, pp. 576–587, Feb. 2023.
[42] F. Mandrile, E. Carpaneto, and R. Bojoi, "Grid-feeding inverter with simplified virtual synchronous compensator providing grid services and grid support," *IEEE Trans. Ind. Appl.*, vol. 57, no. 1, pp. 559–569, Jan./Feb. 2021.
[43] A. Roveri, V. Mallemaci, F. Mandrile, and R. Bojoi, "Power decoupling method for grid inertial support provided by ultra-fast bidirectional chargers," in *Proc. 2023 IEEE Energy Convers. Congr. Expo. (ECCE)*, 2023, pp. 6544–6546.
[44] M. Ebrahimi, S. Ali Khajehoddin, and M. Karimi-Ghartemani, "An improved damping method for virtual synchronous machines," *IEEE Trans. Sustain. Energy*, vol. 10, no. 3, pp. 1491–1500, Jul. 2019.
[45] F. Mandrile, E. Carpaneto, E. Armando, and R. Bojoi, "Simple tuning method of virtual synchronous generators reactive control," in *Proc. 2020 IEEE Energy Convers. Congr. Expo.*, 2020, pp. 2779–2785.
[46] V. Mallemaci, F. Mandrile, E. Carpaneto, and R. Bojoi, "Simplified virtual synchronous compensator with grid–forming capability," *IEEE Trans. Ind. Appl.*, vol. 59, no. 5, pp. 6203–6219, Sep./Oct. 2023.
[47] M. Liserre, F. Blaabjerg, and S. Hansen, "Design and control of an LCL-filter-based three-phase active rectifier," *IEEE Trans. Ind. Appl.*, vol. 41, no. 5, pp. 1281–1291, Sep./Oct. 2005.
[48] M. K. De Meerendre, E. Prieto-Araujo, K. H. Ahmed, O. Gomis-Bellmunt, L. Xu, and A. Egea-Àlvarez, "Review of local network impedance estimation techniques," *IEEE Access*, vol. 8, pp. 213647–213661, 2020.
[49] F. Mandrile, V. Mallemaci, E. Carpaneto, and R. Bojoi, "Lead-lag filter-based damping of virtual synchronous machines," *IEEE Trans. Ind. Appl.*, vol. 59, no. 6, pp. 6900–6913, Nov./Dec. 2023.

ALESSANDRO ROVERI (Student Member, IEEE) received the B.Sc. and M.Sc. degrees in electrical engineering in 2016 and 2019, respectively from Politecnico di Torino, Turin, Italy, where he is currently working toward the Ph.D. degree in electrical engineering.

He joined the Power Electronics Innovation Center (PEIC), Politecnico di Torino, in 2022. He has been an R&D engineer with the company Prima Electro S.p.A., Moncalieri (TO), Italy, since 2018. He is focusing his research activity on the control of grid-connected power converters, virtual synchronous machines and ultra-fast charging systems.

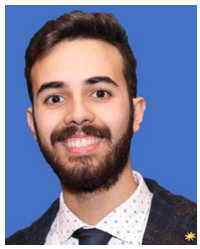

VINCENZO MALLEMACI (Member, IEEE) was born in Messina, Italy, in 1996. He received the bachelor's and master's degrees both in electrical engineering in 2018 and 2020, respectively, from Politecnico di Torino, Torino, Italy, where he received the Ph.D. degree in electrical engineering with Dipartimento Energia "G. Ferraris", in 2024.

His Ph.D. activity focused on virtual synchronous machines and control for power electronic grid–connected converters.

FABIO MANDRILE (Member, IEEE) received the M.Sc. and Ph.D. degrees in electrical engineering from Politecnico di Torino, Torino, Italy, in 2017 and 2021, respectively.

His main research interests include virtual synchronous generators, power electronics for grid-connected applications, the experimental characterization of converters, and motor drives.

RADU BOJOI (Fellow, IEEE) received the M.Sc. degree in electrical engineering from the Technical University of Iasi, Iasi, Romania, in 1993, and the Ph.D. degree in electrical engineering from the Politecnico di Torino, Turin, Italy, in 2002.

He is currently a Full Professor of power electronics and electrical drives with the Energy Department "G. Ferraris" and the Chairman of the Power Electronics Innovation Center, Politecnico di Torino. He has authored or coauthored more than 200 papers covering electrical drives and power electronics for industrial applications, transportation electrification, power quality, and home appliances. He is involved in many research projects with industry aiming at obtaining new products involving emerging technologies.

Dr. Bojoi is past Co-Editor-In-Chief of IEEE TRANSACTIONS ON INDUSTRIAL ELECTRONICS. He is the recipient of six IEEE paper awards.